

## Anisotropic excitonic effects in the energy loss function of hexagonal boron nitride

S. Galambosi,<sup>1,\*</sup> L. Wirtz,<sup>2</sup> J. A. Soininen,<sup>1</sup> J. Serrano,<sup>3</sup> A. Marini,<sup>4,5,6</sup> K. Watanabe,<sup>7</sup> T. Taniguchi,<sup>7</sup> S. Huotari,<sup>1,8</sup> A. Rubio,<sup>6</sup> and K. Hämäläinen<sup>1</sup>

<sup>1</sup>*Department of Physics, P.O. Box 64, University of Helsinki, FI-00014 Helsinki, Finland*

<sup>2</sup>*IEMN, CNRS UMR 8520, Département ISEN, B.P. 60069, F-59652 Villeneuve d'Ascq, France*

<sup>3</sup>*ICREA–Departamento de Física Aplicada, Universitat Politècnica de Catalunya, EPSC, Avenida Esteve Terradas 15, E-08860 Castelldefels, Spain*

<sup>4</sup>*IKERBASQUE, Basque Foundation for Science, E-48011 Bilbao, Spain*

<sup>5</sup>*European Theoretical Spectroscopy Facility (ETSF) and Dipartimento di Fisica, Università di Roma “Tor Vergata,” via della Ricerca Scientifica 1, I-00133 Roma, Italy*

<sup>6</sup>*Nano-Bio Spectroscopy Group, ETSF Scientific Development Centre, Universidad del País Vasco, CFM-CSIC-UPV/EHU-MPC and DIPC, Avenida Tolosa 72, E-20018 San Sebastián, Spain*

<sup>7</sup>*National Institute for Materials Science, 1-1 Namiki, Tsukuba 305-0044, Japan*

<sup>8</sup>*European Synchrotron Radiation Facility, BP 220, F-38043 Grenoble Cedex, France*

(Received 25 January 2011; published 23 February 2011)

The anisotropy of the valence energy-loss function of hexagonal boron nitride (*h*BN) is shown to be largely enhanced by the highly inhomogeneous character of the excitonic states. The energy loss with momentum transfer parallel to the BN layers is dominated by strongly bound, quasi-two-dimensional excitons. In contrast, excitations with momentum transfer perpendicular to the layers are influenced by weakly bound three-dimensional excitons. This striking phenomenon is revealed by a combined study using high-precision nonresonant inelastic x-ray scattering measurements supported by *ab initio* calculations. The results are relevant in general to layered insulating systems.

DOI: [10.1103/PhysRevB.83.081413](https://doi.org/10.1103/PhysRevB.83.081413)

PACS number(s): 78.70.Ck, 71.20.–b, 71.15.–m

Layered hexagonal boron nitride (*h*BN) is the III–V counterpart of graphite. Due to the different electronegativities of boron and nitrogen, it has a large band gap. In recent work<sup>1</sup> it was shown that *h*BN exhibits the potential for lasing at high energies (5.8 eV), making it an attractive candidate for optoelectronic applications in the ultraviolet energy range. Despite its relatively simple crystal structure, *h*BN appears to be a challenge to both experiments and theory. On the experimental side, the challenge is the fabrication of high-quality single crystals, which has been achieved only recently.<sup>2</sup> On the theoretical side, it is well established that the band structure of *h*BN displays an indirect gap<sup>3,4</sup> and the optical absorption spectrum is dominated by correlation effects leading to a strong Frenkel-type excitonic peak at 5.8 eV,<sup>4–6</sup> in agreement with experimental findings.<sup>1</sup> However, the origin of the fine structure of the absorption and luminescence spectra around this peak is still under debate.<sup>7–9</sup> Recent luminescence experiments point toward the role of defects,<sup>10,11</sup> in agreement with the theoretical suggestion in Ref. 7.

In this article, we study the dynamics (dispersion) of the valence excitations of *h*BN using nonresonant inelastic x-ray scattering (NRIXS). Compared to electron energy loss spectroscopy (EELS), NRIXS is better suited for studying the dispersion of low-lying excitations also beyond the first Brillouin zone (1st BZ). This has been used numerous times in the past (see, e.g., Refs. 12 and 13) and provides important new information on the properties of excitations at sub-unit-cell length scales.<sup>14</sup> When studying longitudinal excitations one often finds nonparabolic dispersions<sup>15</sup> and periodicity for low-energy plasmons.<sup>16,17</sup>

We show detailed experimental results on the dispersion of various features and plasmons for the momentum transfer  $\mathbf{q}$  in different crystallographic directions. The loss features show

a strong directional dependence in the comparison not only of in-plane versus out-of-plane but also of different directions within the plane. The origin of the different spectral features and their direction and momentum dependence are analyzed by *ab initio* calculations. Beyond the well-known anisotropy of the electronic band structure, we find, surprisingly, that also the electron-hole interaction has a strong anisotropy. Taking this anisotropy into account may be important in layered materials in general.

The sample was a colorless and transparent single-crystal *h*BN platelet about 700  $\mu\text{m}$  wide and 70  $\mu\text{m}$  thick.<sup>18</sup> The  $\Gamma A$  direction was found to be very nearly parallel to the normal of the platelet. We used single-crystal x-ray diffraction to verify that the sample exhibited an *AB*-type stacking, thus ruling out other stable or metastable stacking sequences.<sup>19,20</sup>

NRIXS spectra were measured on ID16 at the European Synchrotron Radiation Facility, Grenoble, France. The experiment was carried out using the electron volt–resolution spectrometer.<sup>21,22</sup> An energy resolution of 0.6 eV was determined from the FWHM of the quasielastic line. Measurements were performed using the inverse scan technique.<sup>23</sup> The momentum transfer resolution was  $\Delta q/q \approx 0.17$  near the  $K$  point.

The valence bands and the lowest conduction bands of *h*BN can be characterized in terms of the  $\sigma$  and  $\pi$  states of the isolated hexagonal boron nitride sheet. At low momentum transfer the low-energy-transfer structures of the loss function can be divided into transitions between states with the same parity ( $\sigma$ – $\sigma^*$ ,  $\pi$ – $\pi^*$ ) when the momentum transfer is in the plane and states with different parity ( $\pi$ – $\sigma^*$ ,  $\sigma$ – $\pi^*$ ) for momentum transfer along the  $c$  axis.<sup>24</sup> The strong anisotropy in the electronic response can also be seen in the difference for the dielectric constants  $\epsilon_\infty$  parallel and perpendicular to

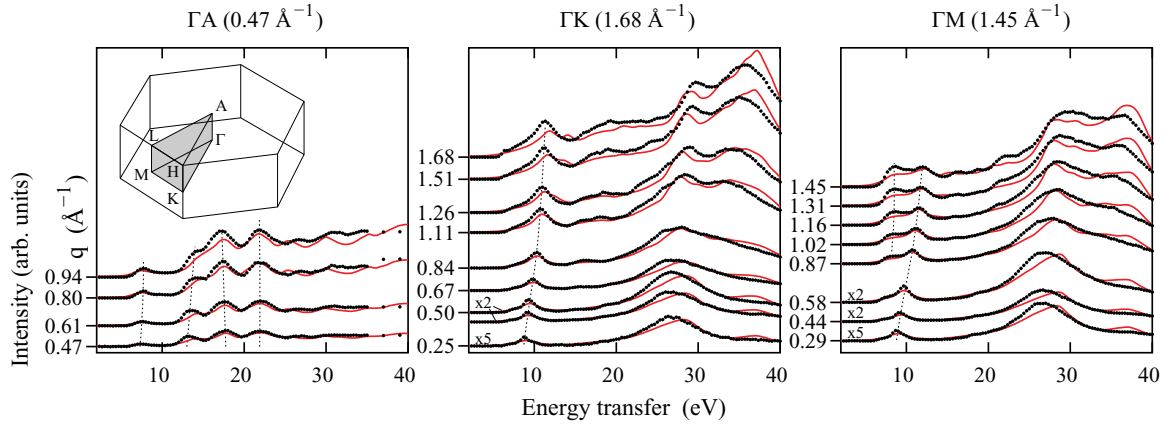


FIG. 1. (Color online) Experimental [filled (black) dots] and theoretical (red/gray lines) NRIXS spectra for low values of momentum transfer along three crystallographic directions. The distance from  $\Gamma$  to the border of the 1st BZ along each direction is indicated in the labels. The  $q^2$ -weighed spectra are vertically displaced proportionally to the value of momentum transfer, which is indicated on the vertical axis. Dashed lines are guides for the eye for features discussed in the text. Inset: 1st BZ of *h*BN, with the irreducible part shaded.

the planes (4.40 and 2.53, respectively).<sup>4</sup> Theoretical NRIXS spectra have been calculated at the level of the random-phase approximation (RPA) starting with Kohn-Sham wave functions obtained within density-functional theory (DFT) in the local-density approximation (LDA).<sup>25</sup> The dielectric function is obtained through  $\epsilon_{\mathbf{G},\mathbf{G}'}(\mathbf{q},\omega) = 1 - v(\mathbf{q} + \mathbf{G})\chi_{\mathbf{G},\mathbf{G}'}^0(\mathbf{q},\omega)$ , where  $v(\mathbf{q}) = 4\pi/|\mathbf{q}|^2$  is the Coulomb potential in reciprocal space and  $\chi_{\mathbf{G},\mathbf{G}'}^0(\mathbf{q},\omega)$  is the independent particle polarizability, which is obtained from a sum over transitions from occupied to unoccupied bands.<sup>26</sup>  $\mathbf{G}$  and  $\mathbf{G}'$  denote reciprocal lattice vectors, and  $\mathbf{q}$  is restricted to the 1st BZ.

The loss function  $\sigma(\mathbf{q},\omega)$ , which is the experimentally probed quantity, is obtained from the inverse of the dielectric matrix  $\sigma(\mathbf{q} + \mathbf{G},\omega) = -\text{Im}[\epsilon_{\mathbf{G},\mathbf{G}'}^{-1}(\mathbf{q},\omega)]$ , where  $\mathbf{q} = \mathbf{q} + \mathbf{G}$ . Crystal local-field effects are automatically included by taking into account the off-diagonal elements of  $\epsilon_{\mathbf{G},\mathbf{G}'}$  in the matrix inversion.<sup>27,28</sup> To compare with the experimental loss function, we have used a broadening  $\eta = 0.6$  eV. We have checked that the use of the time-dependent LDA does not give any substantial improvement.

The experimental and theoretical NRIXS spectra along three crystallographic directions for low values of  $q$  are depicted in Fig. 1. Experimental spectra were normalized to the same area as calculated ones. Overall, the calculations reproduce the experimental spectra well. The *ab initio* calculations match the positions of experimental features and their relative weights as well as the momentum transfer dependence. From the figure it is evident that the spectral features along the  $\Gamma A$  direction do not exhibit any significant dispersion. The high anisotropy of *h*BN is clearly reflected in the differences between the spectra in the hexagonal plane ( $\Gamma K$ ,  $\Gamma M$ ) and the spectrum perpendicular to it ( $\Gamma A$ ). For  $q \lesssim 0.6 \text{ \AA}^{-1}$ , the spectra along  $\Gamma K$  and  $\Gamma M$  are nearly identical. However, as the value of  $q$  is increased an anisotropy within the hexagonal plane is clearly observed. In the high-energy range this anisotropy shows up mainly as a different rate of relative spectral weight increase for the feature between 35 and 40 eV. The in-plane anisotropy is most evident in the behavior of the

$\pi$  plasmon. Its energy disperses from 9 eV at low values of momentum transfer to about 12 eV when  $q$  is near the boundary of the 1st BZ. Along  $\Gamma M$  an additional peak around 8 eV develops for  $q > 0.87 \text{ \AA}^{-1}$ , while in the  $\Gamma K$  direction only a weak shoulder is detected. The double-peak structure along  $\Gamma M$  is also visible in  $\text{Im}[\epsilon(\mathbf{q})]$  (not shown). This indicates that the directional anisotropy can be interpreted in terms of interband transitions. Figure 2(a) shows the band structure of *h*BN. For  $\mathbf{q} = \Gamma K$ , the transitions that dominate the plasmon at 12 eV are the ones from the  $\pi$  band at  $A/H$  to the  $\pi^*$  band at  $H/A$ , respectively (red arrows). For  $\mathbf{q} = \Gamma M$ , the dominant transitions are the ones from the  $\pi$  band at  $A/L$  to the  $\pi^*$  band at  $L/A$  (blue arrows). The observed 8-eV transition at  $\mathbf{q} = \Gamma M$  originates from a  $\pi$ - $\pi^*$  interband transition from  $L$  to a neighboring high symmetry point,  $L'$ . This is marked by the vertical green arrow in Fig. 2(a), even though it is not a vertical transition but one with a momentum difference of  $\mathbf{q} = \Gamma M$ .

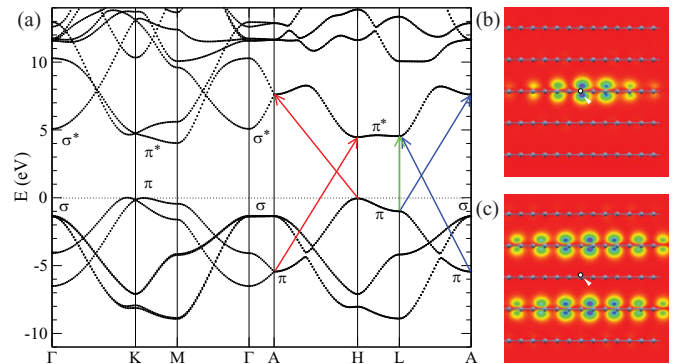


FIG. 2. (Color online) (a) DFT-LDA band structure of *h*BN. (b, c) Two-dimensional projections of the electron probability density  $|\Psi^\lambda(r_h, r_e)|^2$  for the lowest bright exciton in the optical absorption spectrum are shown with  $\mathbf{q} \rightarrow 0$  (b) parallel and (c) perpendicular to the *h*BN planes. The hole position  $r_h$  (marked by the white circle and arrow) is fixed 0.4 a.u. above a nitrogen atom. Balls and sticks indicate atomic layers. Calculations of the excitonic wave functions were performed using the BSE.

At  $\mathbf{q} = \Gamma K$  the plasmon peak around 8 eV is missing because the joint density of states displays only a minor peak there.

To align with the low-energy experimental features the  $\Gamma M$  and  $\Gamma K$  theoretical spectra have been blueshifted by 0.8 eV, whereas for the  $\Gamma A$  spectra a blueshift of 1.5 eV was used. These shifts reflect the well-known fact that the DFT band structure usually underestimates the transition energies between occupied and unoccupied bands. For *hBN* it was shown<sup>3,4,7</sup> that electron-electron correlation, calculated on the level of the GW approximation, increases the transition energies by about 2 eV with respect to DFT-LDA calculations. At the same time, the attractive electron-hole interaction reduces the transition energy such that the difference between experimental and theoretical NRIXS spectra is less than 2 eV. We note that the GW correction alone cannot explain the observed anisotropic shift since  $\pi$  and  $\sigma$  bands are renormalized in the same way. Therefore the experimental NRIXS data cannot be explained with single-particle theories, and the explicit inclusion of electron-hole interaction is necessary.

To check if the combined effect of electron-electron and electron-hole interaction does indeed explain the (anisotropic) shift of the RPA spectra, we carried out parameter-free calculations at selected momentum transfers including excitonic effects on the level of the Bethe-Salpeter equation (BSE).<sup>29</sup> We used the approach of Refs. 15 and 30 and converged all the relevant parameters.<sup>31</sup> To approximate the quasiparticle band energies in Ref. 7, we used a “scissor” of 1.92 eV to shift the LDA conduction band energies, and a small stretch of 5% was applied to the valence bands. As shown in Fig. 3 the BSE results agree well with the experimental and the blueshifted RPA spectra. The slight differences between the two calculations seem to originate mainly from different weights of various spectral features. Also, it should be noted that (except for the energy shift), no extra features seem to arise in the BSE results in comparison with the RPA calculations. This confirms that the RPA successfully describes long-range excitations even in strongly anisotropic and layered materials like *hBN*, with the BSE leading to only minor corrections. Electron-hole effects can alter extended excitations only when the attraction is very strong, as in a wide-gap insulator such as LiF.<sup>29</sup>

Thus we find that due to the layered structure of *hBN*, not only the electronic structure but, importantly, also the electron-hole interaction is highly anisotropic. This is

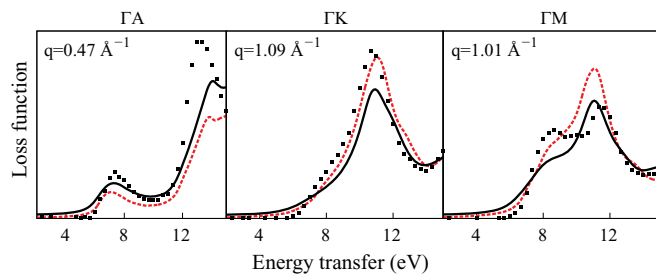


FIG. 3. (Color online) Comparison of the current RPA calculations [solid (black) curve] with a BSE calculation [dashed (red/gray) curve] at selected momentum transfers. RPA spectra are blueshifted as discussed in the text. Experimental data are also shown (black squares).

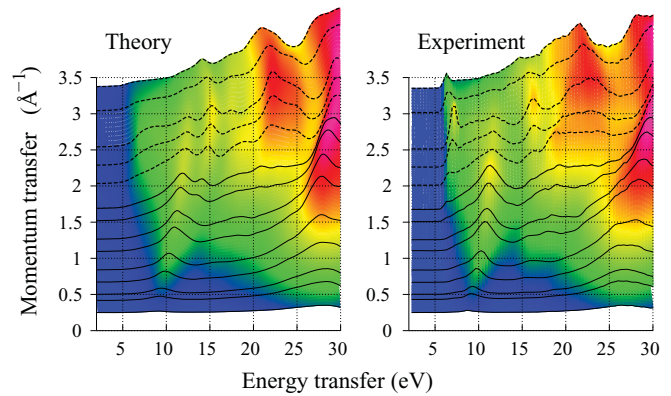


FIG. 4. (Color online) Theoretical RPA (left) and experimental (right) NRIXS spectra, with the momentum transfer directed along the  $\Gamma K$  direction using several values of  $q$ . Spectra for which  $\mathbf{q}$  lies outside the 1st BZ are shown by dashed lines.

elaborated in Figs. 2(b) and 2(c), where we show the excitonic “wave functions” for the lowest visible excitations in the optical absorption spectrum. For  $q$  parallel to planes ( $q_{\parallel}$ ), electron and hole are localized within one plane, forming a strongly bound quasi-two-dimensional compound.<sup>4,7</sup> For  $q$  perpendicular ( $q_{\perp}$ ), electron and hole are localized on different layers and form a more weakly bound three-dimensional compound. This leads to a higher exciton binding energy for  $q_{\parallel}$  than for  $q_{\perp}$  and thus explains why the upshift due to the combined electron-electron and electron-hole interaction is lower for  $q_{\parallel}$  than for  $q_{\perp}$ .

The NRIXS spectra with a larger range of momentum transfers directed along  $\Gamma K$  are displayed in Fig. 4. For most parts the calculated spectra agree well with the experimental ones. The prominent peak dispersing between 25 and 30 eV in the experimental spectra is reproduced very well by the calculations throughout the measured range of momentum transfers. At high momentum transfers ( $>2 \text{ \AA}^{-1}$ ) a new peak showing a small dispersion appears just above 20 eV. Its appearance and dispersion are reproduced well by the calculation. In the same momentum transfer range the calculation shows a peak at around 15 eV that, in the experiments, appears to be less well pronounced and a few electron volts higher in energy. At about 7 eV in the high-momentum-transfer experimental spectra a sharp peak is observed, which is not reproduced by our RPA and BSE calculations. The origin of this peak is still to be understood.

In conclusion, we have observed an anisotropic electron-hole interaction in *hBN*. For  $q_{\parallel}$  the electron and hole tend to form a strongly bound quasi-two-dimensional compound, while for  $q_{\perp}$  the electron and hole tend to be localized on different layers and form a weakly bound three-dimensional compound. This coexistence of two- and three-dimensional excitons is the reason for the anisotropy of 0.7 eV in the energy shift of loss-function calculations on the level of many-body perturbation theory (including excitonic effects) compared to standard calculations on the level of the independent-particle model. Additionally, the observed anisotropic splitting of the  $\pi$  plasmon has been explained as a band structure effect arising from the anisotropic dispersion of the  $\pi$  bands.

This work was supported by the Academy of Finland (Grant No. 1127462/110571), the Spanish MEC (Grant No. FIS2007-65702-C02-01), Grupos Consolidados UPV/EHU del Gobierno Vasco (Grant No. IT-319-07), the European Community through the e-I3 ETSF project (Grant No. GA 211956). J.A.S. benefited from the CMS Network

RIXS collaboration supported by the U S DoE (Grant No. DE-FG02-08ER46540). L.W. acknowledges funding by the ANR through Project No. ANR-09-BLAN-0421-01. A.R. and L.W. benefited from discussions and collaborations with Professor T. Pichler. Computing time was provided by the Red Española de Supercomputación and IDRIS (Project No. 091827).

\*Corresponding author: szabolcs.galambosi@helsinki.fi

- <sup>1</sup>K. Watanabe, T. Taniguchi, and H. Kanda, *Nat. Mat.* **3**, 404 (2004).  
<sup>2</sup>T. Taniguchi, K. Watanabe, and S. Koizumi, *Phys. Status Solidi A* **201**, 2573 (2004).  
<sup>3</sup>X. Blase, A. Rubio, S. G. Louie, and M. L. Cohen, *Phys. Rev. B* **51**, 6868 (1995).  
<sup>4</sup>B. Arnaud, S. Lebègue, P. Rabiller, and M. Alouani, *Phys. Rev. Lett.* **96**, 026402 (2006).  
<sup>5</sup>L. Wirtz, A. Marini, and A. Rubio, *Phys. Rev. Lett.* **96**, 126104 (2006).  
<sup>6</sup>A. Marini, *Phys. Rev. Lett.* **101**, 106405 (2008).  
<sup>7</sup>L. Wirtz, A. Marini, M. Grüning, C. Attaccalite, G. Kresse, and A. Rubio, *Phys. Rev. Lett.* **100**, 189701 (2008).  
<sup>8</sup>B. Arnaud, S. Lebègue, P. Rabiller, and M. Alouani, *Phys. Rev. Lett.* **100**, 189702 (2008).  
<sup>9</sup>K. Watanabe and T. Taniguchi, *Phys. Rev. B* **79**, 193104 (2009).  
<sup>10</sup>P. Jaffrennou, J. Barjon, J.-S. Lauret, B. Attal-Trétout, F. Ducastelle, and A. Loiseau, *J. Appl. Phys.* **102**, 116102 (2008).  
<sup>11</sup>L. Museur, E. Feldbach, and A. Kanaev, *Phys. Rev. B* **78**, 155204 (2008).  
<sup>12</sup>W. A. Caliebe, J. A. Soininen, E. L. Shirley, C.-C. Kao, and K. Hämäläinen, *Phys. Rev. Lett.* **84**, 3907 (2000).  
<sup>13</sup>G. G. Fuentes, E. Borowiak-Palen, T. Pichler, X. Liu, A. Graff, G. Behr, R. J. Kalenczuk, M. Knupfer, and J. Fink, *Phys. Rev. B* **67**, 035429 (2003).  
<sup>14</sup>P. Abbamonte, T. Graber, J. P. Reed, S. Smadici, C. L. Yeh, A. Shukla, J. P. Rueff, and W. Ku, *Proc. Natl. Acad. Sci. USA* **105**, 12159 (2008).  
<sup>15</sup>J. A. Soininen and E. L. Shirley, *Phys. Rev. B* **61**, 16423 (2000).  
<sup>16</sup>S. Galambosi, J. A. Soininen, A. Mattila, S. Huotari, S. Manninen, G. Vankó, N. D. Zhigadlo, J. Karpinski, and K. Hämäläinen, *Phys. Rev. B* **71**, 060504 (2005).  
<sup>17</sup>Y. Q. Cai *et al.*, *Phys. Rev. Lett.* **97**, 176402 (2006).  
<sup>18</sup>Y. Kubota, K. Watanabe, O. Tsuda, and T. Taniguchi, *Science* **317**, 932 (2007).

- <sup>19</sup>L. Liu, Y. P. Feng, and Z. X. Shen, *Phys. Rev. B* **68**, 104102 (2003).  
<sup>20</sup>N. Ooi, A. Rairkar, L. Lindsley, and J. B. Adams, *J. Phys. Condens. Matter* **18**, 97 (2006).  
<sup>21</sup>S. Huotari, G. Vankó, F. Albergamo, C. Ponchut, H. Graafsma, C. Henriquet, R. Verbeni, and G. Monaco, *J. Synchrotron Radiat.* **12**, 467 (2005).  
<sup>22</sup>R. Verbeni, T. Pykkänen, S. Huotari, L. Simonelli, G. Vankó, K. Martel, C. Henriquet, and G. Monaco, *J. Synchrotron Radiat.* **16**, 469 (2009).  
<sup>23</sup>K. Hämäläinen, S. Manninen, C.-C. Kao, W. Caliebe, J. B. Hastings, A. Bansil, S. Kaprzyk, and P. M. Platzman, *Phys. Rev. B* **54**, 5453 (1996).  
<sup>24</sup>C. Tarrío and S. E. Schnatterly, *Phys. Rev. B* **40**, 7852 (1989).  
<sup>25</sup>DFT calculations were performed with ABINIT.<sup>32</sup> Wave functions are expanded in plane waves with an energy cutoff of 25 hartree. The 1s electrons are replaced by Troullier-Martins pseudopotentials. Lattice parameters  $a = 2.504 \text{ \AA}$  and  $c = 6.660 \text{ \AA}$  were used.<sup>33</sup>  
<sup>26</sup>S. L. Adler, *Phys. Rev.* **126**, 413 (1962).  
<sup>27</sup>A. Marini, C. Hogan, M. Grüning, and D. Varsano, *Comput. Phys. Commun.* **180**, 1392 (2009).  
<sup>28</sup>The matrix  $\epsilon_{\mathbf{G},\mathbf{G}'}$  comprises a total of 80  $\mathbf{G}$  vectors in our calculations. The 1st BZ is sampled with a  $60 \times 60 \times 4k$ -point grid for the calculations with  $q$  parallel to the hexagonal plane and with a  $30 \times 30 \times 12$  grid for calculations with  $q$  perpendicular to it. We have included 8 occupied and 52 unoccupied bands, up to an energy of 70 eV above the valence band maximum. Calculations were performed with YAMBO.<sup>27</sup>  
<sup>29</sup>G. Onida, L. Reining, and A. Rubio, *Rev. Mod. Phys.* **74**, 601 (2002).  
<sup>30</sup>L. X. Benedict and E. L. Shirley, *Phys. Rev. B* **59**, 5441 (1999).  
<sup>31</sup>A  $k$ -space grid of  $24 \times 24 \times 12$ , a  $\mathbf{G}$  grid of  $5 \times 5 \times 5$  and 32 unoccupied bands were used in these calculations. Finally, a broadening of 0.4 eV was applied for the comparison.  
<sup>32</sup>X. Gonze *et al.*, *Comp. Mat. Sci.* **25**, 478 (2002).  
<sup>33</sup>V. L. Solozhenko, G. Will, and F. Elf, *Solid State Commun.* **96**, 1 (1995).